

Calibration for multiple motion errors of X-Y table on micro-coordinate measuring machine (M-CMM) by utilizing multi-probe scanning method

Ping Yang¹, Tomohiko Takamura¹, Satoru Takahashi¹, Kiyoshi Takamasu¹,
Osamu Sato², Sonko Osawa², and Toshiyuki Takatsuji²

¹ Department of Precision Engineering, The University of Tokyo, Tokyo, Japan

² National Metrology Institute of Japan, National Institute of Advanced Industrial Science and Technology, Ibaraki, Japan

Abstract—A high-precision micro-CMM (M-CMM) is currently under development in the National Institute of Advanced Industrial Science and Technology (AIST), in collaboration with the University of Tokyo. Our aim is to achieve 50-nm measurement uncertainty with a measuring volume of $30 \times 30 \times 10$ mm (XYZ). In this paper, we have designed a multi-probe scanning system to calibrate the multiple motion errors of X-Y table stage on the M-CMM and measure the profile of a reference bar mirror simultaneously. In the scanning system, three laser interferometers probe the surface of the flat bar mirror which is fixed on top of the X-Y table stage, while the autocollimator simultaneously measures the yaw error of the moving axis. We have discussed the simulation results of the uncertainty value of the multi-probe scanning method and conducted pre-experiments based on a stepping motor system to verify the simulation results. The results from the pre-experiment verify that the multi-probe measurement method performs the yaw and straightness motion error measurement extremely well and also measure the reference bar mirror profile with a small standard deviation of 10 nm. Finally, we are going to perform experiments on the M-CMM to calibrate the multiple motion errors of X-Y table stage in near future.

Key Words: Micro-CMM, multi-probe scanning method, uncertainty, motion errors, profile

1. Introduction

In modern microsystem technologies, requirements for three-dimensional (3D) metrologies for microsystem components have increased. However, conventional measuring methods cannot meet these requirements because the measurement scales of conventional coordinate measuring machines (CMMs) are usually limited to several tens of millimeters or more, which is not suitable for measuring small parts of the order of submillimeters or even submicrometers. In addition, conventional CMMs lack good 3D measurement uncertainty levels and are often not supplied with the proper probing systems in many applications [1]. Therefore, different kinds of micro-CMMs equipped with special micro-probe systems for 3D metrology having high-aspect-ratio micro parts are currently being developed to satisfy the described requirements.

IBS Precision Engineering has developed the Isara CMM, an ultra-precision 3D coordinate measuring machine, with a measuring volume of $100 \times 100 \times 40$ mm and a 3D measuring uncertainty of 30 nm [2]. The F25 micro-CMM (Carl Zeiss) is another commercially available product with a measuring volume of one cubic decimeter and measuring uncertainty of 250 nm at a resolution of 7.5 nm [3]. Further, the National Physical Laboratory (NPL) is currently conducting researches into developing a micro-scale probe that promises the full potentials of micro-CMMs [4]. The Physikalisch-Technische Bundesanstalt (PTB) is working along with Carl Zeiss in the field of 3D measurements on micro parts with measurement uncertainties in the range of less than $0.1 \mu\text{m}$ [5]. M-NanoCoord designed by Mitutoyo can equip with vision probe system and touch probe system with a measuring volume of $200 \times 200 \times 100$ mm and accuracy over 200 nm [6].

A high-precision micro-CMM (M-CMM) is currently under development at the National Metrology Institute of Japan in the National

Institute of Advanced Industrial Science and Technology (AIST), in collaboration with the University of Tokyo. The moving volume of the M-CMM is $160 \times 160 \times 100$ mm (XYZ), and our aim is to achieve 50-nm measurement uncertainty with a measuring volume of $30 \times 30 \times 10$ mm (XYZ). Since the motion errors of each stage of the M-CMM should be calibrated and compensated in order to develop a high precision M-CMM, we have proposed a multi-probe scanning method, simulated its measurement uncertainty results, and discussed its applications for evaluating the multiple motion errors of each stage and measuring the profile of a reference bar mirror [7–9].

2. M-CMM configuration

The M-CMM configuration comprises three main parts: a cross XY-axis, a Z-axis, and a probe unit. Each axis has a linear motion stage system that comprises air-bearing sliders, a glass linear scale, a moving table, a driving motor, and related parts.

There are three special specifications in the M-CMM design. The frame table and main structure of each axis is made of alumina ceramic having high rigidity and low coefficient of thermal expansion (CTE; 7 ppm/K). Further, the base plate of the M-CMM is made of granite having CTE of 5 ppm/K, as shown in Fig. 1. In general, thermal effects are one of most significant reasons of non-repeatability in measuring machine accuracy. The M-CMM minimizes these effects by using the same alumina ceramic materials. Because of this optimized design, when the temperature changes, the main mechanical structures will deform almost in the same deviation range. On the other hand, the measurement area is covered with an enclosure to minimize heat inputs from the machine environment (e.g., from operators). Therefore, the M-CMM exhibits good performance in response to temperature changes, and thermal deformations due to the driving heat and temperature changes are significantly reduced.

We subsequently divided the XYZ-axis into two mechanical parts: the XY-axis, which is stacked with two linear stages, and the Z-axis, which is separately designed and constructed at the center of the frame table. The primary reason for this division is that the measurement uncertainties of the Z-axis are larger than those of the XY-axis because the sensitivity of the 3D contacting micro-probes in the Z-direction is usually lower than that in the XY plane; this, in turn, is due to the effect of the length of the probe stylus on the horizontal probing direction.

Finally, the probe unit has a changeable connector, and hence, the M-CMM can use different types of touch probe systems and conduct 3D measurements with different levels of uncertainties.

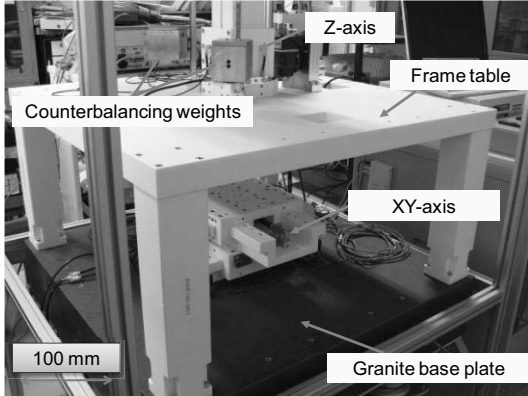


Fig. 1 Main structure of micro-coordinate measuring machine (M-CMM)

3. Calibration for motion errors of X-Y table stage

The XY-axis is a stacking-type mechanism having two linear stages comprising air-bearing sliders, ultrasonic motors (linear motors), moving tables, linear scales, and related parts, as shown in Fig. 2. The X-Y table stage is fixed on a granite base plate. Each stage of the XY-axis is driven by an ultrasonic motor, and its movement is detected by a linear scale mounted on the side of the moving stage. A moving table with a size of 280 mm × 280 mm has sufficient space to perform calibrations.

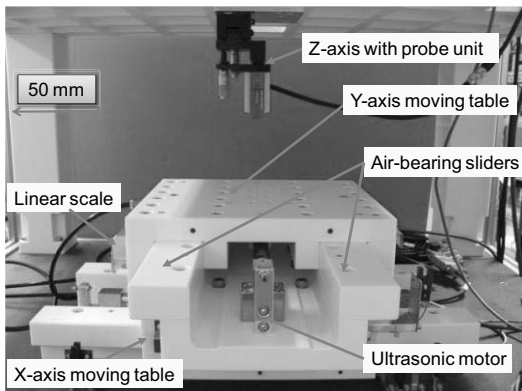


Fig. 2 Structure of XY stage and probe unit

Because of the mechanical design of X-Y table stage, we cannot satisfy the Abbe principle, and the Abbe error will exist. The Abbe errors are caused by the rotational errors of relative translations between the

reference and sensing points; the Abbe offsets are the distances between the reference and sensing points. The Abbe errors are often the most important uncertainty sources in dimensional metrology applications that require measurement uncertainties of only a few nanometers

The motion errors of the M-CMM without any compensation are shown in Table 1. For instance, when the Abbe offset H is 50 mm, if the tilt of the X axis, θ , to be 8 μrad , the Abbe error δ in the X direction will be 400 nm (Fig. 3). It cannot meet our expectation of 50-nm measurement uncertainty. Therefore, the 6 DOFs of each stage of the M-CMM are very important factors in the development of a high-precision M-CMM. Hence, the motion errors of the XY stage in the M-CMM should be measured and calibrated.

Table 1: Motion errors of M-CMM without compensation

Axis	Degrees of freedom	Accuracy / range
X,Y	Translation	Max: 0.5 μm / 160mm
X,Y	Rotation	Max: 8 μrad / 160 mm
Z	Translation	Max: 0.3 μm / 100 mm
Z	Rotation	Max: 5 μrad / 100 mm

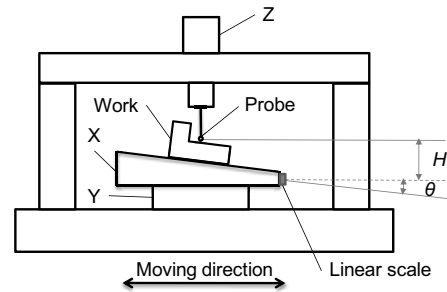


Fig. 3 Illustration of Abbe error without calibration

In the traditional calibration method, one displacement sensor is used with a high-accuracy reference bar mirror. The accuracy of this method is dependent on the accuracy of the reference mirror because the final measured results include the profile of the reference bar mirror. In this paper, we have designed a multi-probe scanning system to calibrate the multiple motion errors of X-Y table stage on the M-CMM and measure the profile of a reference bar mirror simultaneously.

4. Measurement Principle

4.1 Principle of multi-probe scanning method

The principle of the multi-probe scanning method is based on an error separation technique originally proposed by Whitehouse in 1976 [10] and widely used in the precision measurement field [11–12]. Multi-probe methods for measuring straightness and roundness have been extensively developed. These methods began with research into sequential two-point and three-point methods [12–13] that not only measure the straightness motion error of the guideway, but also the straightness of the objective surface. However, these methods are limited in terms of horizontal resolution, and the results are affected by systematic and random errors of the output sensors. In order to improve these, a multi-probe scanning method comprising three laser interferometers and one autocollimator has been proposed and analyzed. In the multi-probe scanning system, the laser interferometers probe the

surface of a flat bar mirror that is fixed on top of an X-Y scanning stage, while the autocollimator simultaneously measures the yaw error of the scanning stage [7]. Unlike the case where the displacement sensors are fixed on a moving scanner, the laser interferometers are mounted on stationary housings, as shown in Fig. 4. During the measurement, the scanning stage moves in steps. And at each step, a computer automatically collects the data from the laser interferometers and the autocollimator. Let the corresponding laser interferometers and autocollimator outputs be $m_1(n)$, $m_2(n)$... $m_M(n)$ and $m_a(n)$. They can be expressed as follows:

$$\begin{cases} m_1(n) = f(x_n) + e_1(n) \\ m_2(n) = f(x_n + D_1) + e_1(n) + D_1 \cdot e_2(n) + c_2 \\ m_3(n) = f(x_n + D_2) + e_1(n) + D_2 \cdot e_2(n) + c_3 \\ m_a(n) = e_2(n) \end{cases} \quad (1)$$

Here $f(x_n)$ denotes the flat bar mirror profile; $e_1(n)$ and $e_2(n)$ denote horizontal straightness motion and yaw errors with systematic and random errors at the first step, respectively at each step n ; D_1 is the installation distance between the 1st and 2nd laser interferometers; D_2 is the installation distance between the 1st and 3rd laser interferometers; and c_2 and c_3 are supplementary parameters that are defined by $c_j = u_j - u_1 - D_{j-1} \cdot u_a$, $j = 2, 3$. The parameters u_1 , u_2 , u_3 and u_a are the offsets of each probe. The number of sampling points of the flat bar mirror profile is N and the number of sampling points of the motion errors is given by $N_s = N - d_2$. The parameter d_2 is defined as $d_2 = D_2/s$ that is the normalized distance of the 3rd laser interferometer. The measuring step distance of the scanning stage is s and $L = n \times s$ specifies the moving scale of the stage, as shown in Fig. 4. For the analysis here, the step distance s is determined by the number of the laser interferometers and their relative distances.

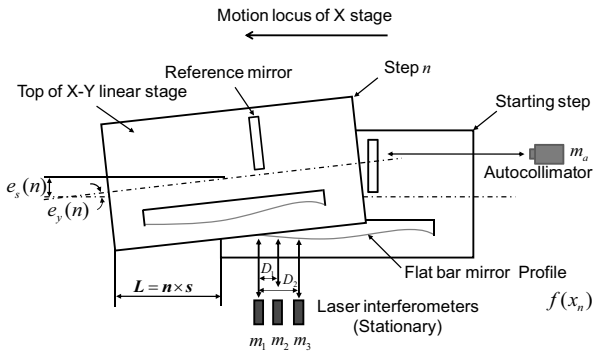


Fig. 4 Principle of multi-probe scanning method

4.2 Data processing based on simultaneous linear equations and least-squares method

From Eq. (1), the whole measurement process is expressed simply as a set of simultaneous linear equations,

$$\mathbf{Y} = \mathbf{A}\mathbf{X} \quad (2)$$

where \mathbf{Y} denotes the measured vectors

$$\mathbf{Y} = [m_1(1), \dots, m_1(N), \dots, m_2(1), \dots, m_2(N), \dots, m_3(1), \dots, m_3(N), \dots, m_a(1), \dots, m_a(N)]^T \quad (3)$$

and \mathbf{A} is the Jacobian matrix constructed by the differential of \mathbf{Y} and \mathbf{X} . The unknown vectors \mathbf{X} are the flat bar mirror profile and the motion errors.

$$\mathbf{X} = [f(x_1), \dots, f(x_{N-2}), e_1(1), \dots, e_1(N_s), e_2(1), \dots, e_2(N_s), c_2, c_3]^T \quad (4)$$

For a solution of the matrix \mathbf{X} to exist according to Eq. (2), two additional conditions must be satisfied. One is $N_s \geq D_2/s$, which means that the number of sampling points of the motion errors is greater than or equal to the normalized distance of the 3rd laser interferometer. The least-squares solution exists when this condition is met. The other is the greatest common divisor (GCD) of d_1 and d_2 should be 1. (GCD(d_1, d_2) = 1) The parameters D_1 , D_2 , and s are chosen to satisfy these conditions.

From Eq. (2), the objective model \mathbf{Y} comprises a linear combination of the parameters \mathbf{X} . In the measurement system, \mathbf{Y} is assumed to have random errors. The sources of error for each measured vector, which follow the normal distribution, are dependent. Utilizing the linear least-squares method to calculate the unknown matrix \mathbf{X} , we obtain

$$\mathbf{X} = (\mathbf{A}^T \mathbf{S}^{-1} \mathbf{A})^{-1} \mathbf{A}^T \mathbf{S}^{-1} \mathbf{Y} \quad (5)$$

where \mathbf{S} denotes the error variance between each measurement point.

From the reconstruction procedure, the measurement uncertainty associated with the reconstructed vectors \mathbf{X} can be derived. The reliability of the reconstructed data and its associated measurement uncertainty can be assessed via a criterion. The associated uncertainty of the measurement process is calculated via the error propagation matrix \mathbf{S}_X that is deformed in the least-squares method, as shown in Eq. (6). The vectors on the diagonal of \mathbf{S}_X are the square values of the measurement uncertainties of the flat bar mirror profile from 1 to $N-2$.

$$\mathbf{S}_X = (\mathbf{A}^T \mathbf{S}^{-1} \mathbf{A})^{-1} = \begin{pmatrix} r_{11} & \dots & r_{1Q} \\ \vdots & \ddots & \vdots \\ r_{Q1} & \dots & r_{QQ} \end{pmatrix}, \quad (6)$$

5. Uncertainty Simulation

In the simulation, we begin by setting up simultaneous linear equations that express the linear relationship between the measured parameters and the unknowns. We then analyze the measurement uncertainty for the flat bar mirror profile and calculate the unknown parameters by applying the least-squares method [15]. We set up three laser interferometers and one autocollimator in the simulation model. For the simulation, $f(x_n)$ is predefined; $e_1(n)$ and $e_2(n)$ are

random numbers from the initialization; L is set to 100 mm; and the standard deviation of the laser interferometers and autocollimator were set to $\sigma_1 = \sigma_2 = \sigma_3 = 3.5$ nm and $\sigma_a = 0.23$ μ rad. These values were taken from the model specifications (laser interferometers: 10705A, Agilent; autocollimator: Elcomat 3000, Moller-Wedel Optical). Each sampling point of $f(x_n)$ is picked by the predefined function. According to the GCD condition, we choose different sets of D_1 and D_2 values, with s set to 1 mm, as shown as Table 2, in order to analyze the factors influencing the measurement uncertainty of the flat bar mirror profile.

Table 2 Different installation distances of laser interferometers

Group	D_1 (mm)	D_2 (mm)
No.1	2	5
No.2	4	9
No.3	5	11
No.4	10	21
No.5	15	31

The simulation results are shown in Fig. 5.

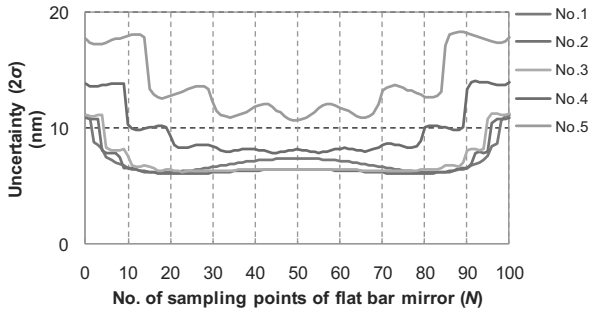


Fig. 5 Relationship between different installation distances of laser interferometers and measurement uncertainty of flat bar mirror profile for $\sigma_1 = \sigma_2 = \sigma_3 = 3.5$ nm and $\sigma_a = 0.23$ μ rad.

Fig. 5 shows the relationship between different sets of installation distances of laser interferometers. From Fig. 5, the uncertainty curves increase almost continuously with increasing installation distance (D_1 , D_2). Thus, the smaller the installation distances, the higher the accuracy. However, it is difficult to arrange the installation distances to be less than 6 mm because the diameter of the laser beam is 6 mm. As a result, we chose group No. 4 ($D_1 = 10$ mm, $D_2 = 21$ mm) for our experiment. The average measurement uncertainty is approximately 10 nm, which is acceptable for nanometer scale measurements.

6. Pre-experiment

6.1 Pre-experiment Setup

The pre-experiment of the multi-probe scanning method has been designed to measure the motion errors of an XY stage based on a stepper motor system. Fig. 6 shows the actual setup of the pre-experiment that consisted of an XY stepper motor stage, laser interferometers, receivers, beam splitters, optical reflection mirrors, and an autocollimator. The optical reflection parts that are fixed on top of the

XY stage consisted of a reference bar mirror, a housing for the reference bar mirror, and a reference mirror for the autocollimator.

The moving direction of the X-axis was from left to right. In the equipment setup, the sampling length of the flat bar mirror is 100 mm because the valid size of the flat bar mirror is approximately 100 mm \times 30 mm with an accuracy of $\lambda = 632.8$ nm. Setting $D_1 = 10$ mm, $D_2 = 21$ mm, and $s = 1$ mm, and for $N = 100$, gives $N_s = N - d_2$ as 79.

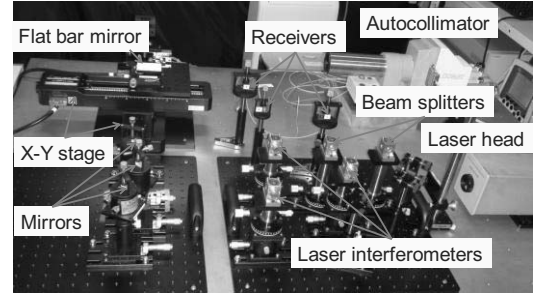


Fig. 6 Actual setup of pre-experiment

6.2 Stability of each sensor

The accuracies of the laser interferometers are sensitive to the measurement environment and other external factors. Therefore, we measured the stability of each sensor at the first sampling point before performing the experiment. The standard deviations of the laser interferometers and the autocollimator were calculated to be $\sigma_1 = \sigma_2 = \sigma_3 = 3.5$ nm, and $\sigma_a = 0.23$ μ rad in 5 minutes that is approximately the same duration as a whole measurement process.

6.3 Pre-experiment results

The yaw errors along the X-axis $e_2(n)$ from ten repetitions of the experiments are presented in Fig. 7. The range of $e_2(n)$ is approximately 40 μ rad. The horizontal straightness motion errors along the X-axis $e_1(n)$, obtained by applying the simultaneous equation and least-squares methods, are shown in Fig. 8. The range of $e_1(n)$ is approximately 2 μ m. The reconstructed profiles of the flat bar mirror $f(x_n)$ are shown in Fig. 9, and the profiles are reproduced well for each of the ten measurements.

The two standard deviation (95%) values of the flat bar mirror profile calculated over the ten experiments are shown in Fig. 10 indicated by the red curve; the average is approximately 10 nm. According to the Fig. 5, the simulated measurement uncertainty (2σ) is shown in Fig. 10 and indicated by the black curve with parameters set as per group No. 4. Comparing these two curves, we conclude that the two standard deviation of the flat bar mirror profile is mainly fitting the range of 2σ . The multi-probe scanning method performs well with a small deviation of 10 nm in the measurement of the flat bar mirror profile, and measures the horizontal straightness motion and yaw errors successfully with a high horizontal resolution. Moreover, in the comparison between the simulated measurement uncertainty ($\pm 2\sigma$) and the difference curves between the average value of ten profiles and each profile (Fig.11), we note that the difference curves mainly lie with ± 10 nm ($\pm 2\sigma$) verifying

nanometer accuracy.

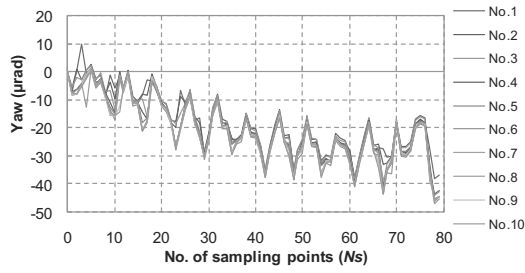


Fig. 7 Yaw error of X stage

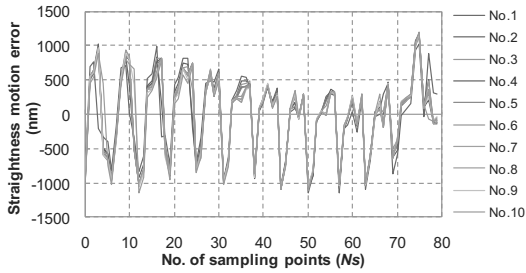


Fig. 8 Straightness motion error of X stage

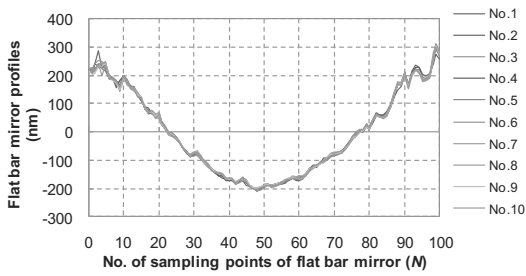


Fig. 9 Profile of flat bar mirror

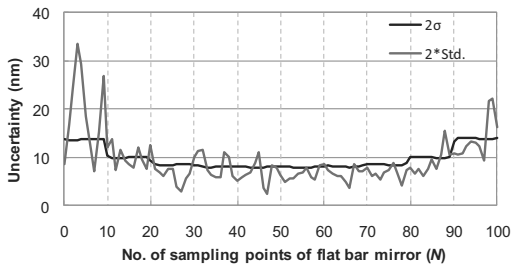


Fig. 10 Comparison of two standard deviations of ten times flat bar mirror profiles (black line) with simulated measurement uncertainty (red line) (2σ)

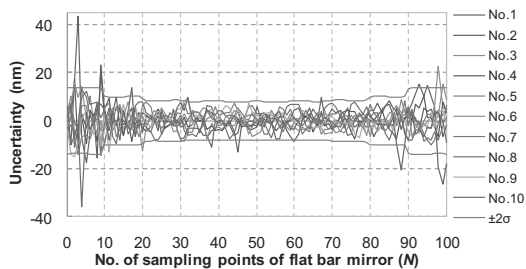


Fig. 11 Comparison of simulated measurement uncertainty ($\pm 2\sigma$) of flat bar mirror profile with difference between average value of ten profiles and each profile

6.4 Comparison with ZYGO's interferometer system

To confirm the measurement accuracy of the flat bar mirror profile, we compared our profile data with results measured by ZYGO's interferometer system. The average flat bar mirror profile for ten experiments is indicated in Fig. 12 by the red curve. The profile measured by the ZYGO's interferometer system is indicated by the black curve. The comparison shows that the two profiles are approximately the same within the deviation range of 10 nm, excluding some points at the edge of the mirror. This is a limitation of the multi-probe scanning method because these points can only be measured by one displacement sensor.

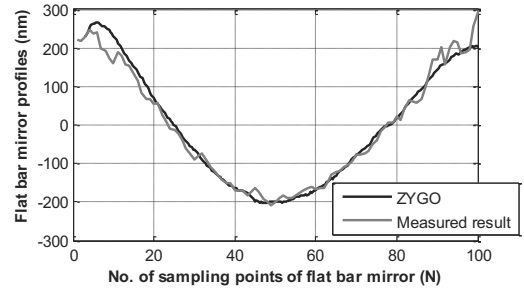


Fig. 12 Comparison of average flat bar mirror profile with profile measured by ZYGO's interferometer system

7. Conclusions and future works

We have devised a multi-probe scanning method to calibrate the multiple motion errors of X-Y table on M-CMM and measure a flat bar mirror profile with nanometer accuracy simultaneously. From the simulation and pre-experiment results, we can make the following conclusions.

- (1) The simulation results indicate that the average measurement uncertainty (2σ) almost continuously with increasing installation distances between the laser interferometers (D_1, D_2). When we set $D_1 = 10$ mm, $D_2 = 21$ mm, $s = 1$ mm, $\sigma_1 = \sigma_2 = \sigma_3 = 3.5$ nm, and $\sigma_a = 0.23$ μ rad, the average measurement uncertainty is approximately 10 nm.
- (2) From the pre-experiment, the two standard deviation of the flat bar mirror profile is mainly fitting the simulated measurement uncertainty of 10 nm (2σ). Moreover, the difference curves between the average value of ten profiles and each profile mainly lie within the simulated measurement uncertainty of ± 10 nm ($\pm 2\sigma$). In addition, the multi-probe scanning system can also measure the yaw and horizontal straightness motion errors successfully with a high horizontal resolution.
- (3) Comparing with the results measured by the ZYGO's interferometer system, there are some variations in the flat bar

mirror profile of our measurement results. They are due to some systematic error sources in the measurement process, such as the accuracy of moving the scanning stage and the misalignment of the optical devices. These error sources will be analyzed in greater detail in M-CMM experiment.

The results from the pre-experiment verify the performance of multi-probe scanning method. Therefore, we have designed and built the optical parts on the M-CMM. Fig. 13 shows the actual optical setup on M-CMM. The laser head is fixed on top of the frame table because the space on granite base plate is limited. Laser light is divided into three paths through the 33% and 50% beam splitters. Other optical devices consisted of several reflection mirrors, laser interferometers, receivers, reference bar mirror, and an autocollimator. Finally, we are going to perform experiments on the M-CMM to calibrate the multiple motion errors of X-Y table stage in near future.

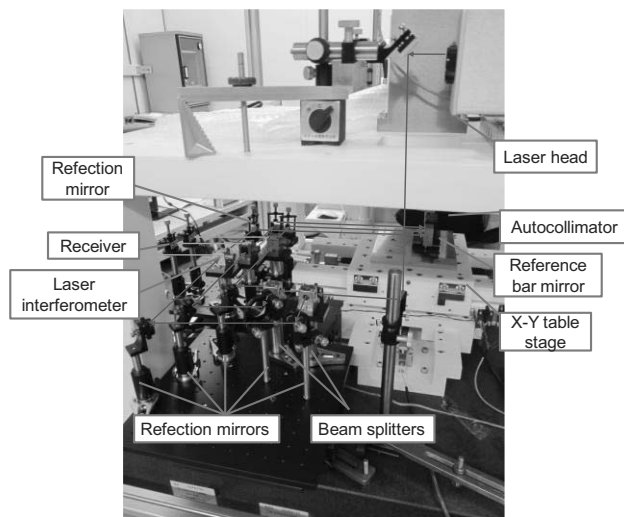


Fig. 13 Actual setup on M-CMM

Acknowledgements

Ping Yang wishes to thank the supports from the Japanese Government (Monbukagakusho: MEXT) Scholarship and Japanese Global COE Program, “Global Center of Excellence for Mechanical Systems Innovation”.

References

[1] Cao S, Brand U, Kleine-Besten T, Hoffmann W H, Schwenke, B'utefisch S, and B'uttgenbach S. Recent developments in dimensional metrology for microsystem components. *Microsyst. Technol.* 2002;8; 3–6

[2] IBS Precision Engineering, ISARA-Ultra Precision Coordinate Measuring Machine, http://www.ibspe.com/ibs_precision_engineering_uk/ibs_isara.html

[3] Carl Zeiss, F25 Microsystem CMM,

<http://www.zeiss.de/4125682000247242/Contents-Frame/5B1A8EBC2A5E14B886257154006AE1A3>

[4] Claverley, J. D, and Leach, R. K. A vibrating microscale CMM probe for measuring high aspect ratio structures. *Microsyst. Technol.* 2010;16; 1507–12

[5] M.Neugebauer, High-precision Calibration of Ball Plates for Micro-Coordinate Measuring Machines, http://www.ptb.de/cms/en/fachabteilungen/abt5/nachrichten5/scientific-news.html?tx_ttnews%5Btt_news%5D=86&tx_ttnews%5BbackPid%5D=752

[6] Mitutoyo, UMAP Vision System, Bulletin No. 1631.

[7] Yang P, Shibata S, Takahashi S, Takamasu K, Sato O, Osawa S, and Takatsuji T. A Multi-Probe Measurement Method to Evaluate the Yaw and Straightness Errors of XY Stage on High Precision CMM. *Key Engineering Materials* 2010; 447–448; 590–594

[8] Yang P, Shibata S, Takahashi S, Takamasu K, Sato O, Osawa S, and Takatsuji T. Development of high precision Coordinate Measuring Machine (CMM) (1st report, Evaluation method of XY stage). 2009; JSPE autumn conference; 725–26

[9] Yang P, Shibata S, Takahashi S, Takamasu K, Sato O, Osawa S, and Takatsuji T. Development of high precision Coordinate Measuring Machine (CMM) (2nd report, Pre-experiment of multi-probe method for evaluating the XY stage). 2010; JSPE spring conference; 377–78

[10] Whitehouse DJ. Some theoretical aspects of error separation techniques in surface metrology. *J. of Phys. E: Sci. Instrum.* 1976; 9; 531–536

[11] Evans CJ, Hocken RJ, and Estler WT. Self-calibration: reversal, redundancy, error separation, and ‘absolute testing’. *Ann. CIRP* 1996; 45 (2); 617–634

[12] Marsh ER, Arneson DA, and Martin DL. A comparison of reversal and multiprobe error separation. *Prec. Eng.* 2010; 34(1); 85–91

[13] Tanaka H, Tozawa K, and Sato H. Application of a new straightness measurement method to large machine tools. *Ann CIRP* 1981; 30(1); 455–9

[14] Makosch G, and Drollinger B. Surface profile measurement with a scanning differential ac interferometer. *Applied Optics* 1984; 23–24; 4544–53

[15] Liu SJ, Watanabe K, Chen X, Takahashi S, and Takamasu K. Profile measurement of a wide-area resist surface using a multi-ball cantilever system. *Prec. Eng.* 2009; 33; 50–55